Available online at www.sciencedirect.com
ScienceDirect
Acta Materialia 59 (2011) 4068–4078
Acta MATERIALIA
www.elsevier.com/locate/actamat

Thermal vacancies in Fe_3Al studied by positron annihilation

J. Čížek *, F. Lukáč, O. Melikhova, I. Procházka, R. Kužel

Faculty of Mathematics and Physics, Charles University in Prague, V Holešovičkách 2, CZ-180 00 Prague 8, Czech Republic

Received 1 October 2010; accepted 10 March 2011
Available online 7 April 2011

Abstract

Vacancies in Fe_3Al intermetallic alloys were investigated by positron annihilation spectroscopy combined with X-ray diffraction. Two complementary techniques of positron annihilation were employed: positron lifetime spectroscopy and coincidence Doppler broadening. The experimental results were combined with ab initio theoretical calculations of positron characteristics. It was found that Fe_3Al quenched from 1000 °C exhibits a mainly disordered A2 structure. Defects in the as-quenched sample were identified as Fe vacancies on the A sub-lattice surrounded by Al nearest neighbors. The concentration of quenched-in vacancies was determined from the positron lifetime results. The samples were subsequently subjected to isochronal annealing which enabled an investigation of the recovery of quenched-in vacancies and the formation of thermal vacancies in B2 phase. It was found that recovery of quenched-in vacancies is accompanied by ordering to the $D0_3$ structure. The enthalpy and entropy of formation were determined for vacancies in the B2 phase.

Keywords: Iron aluminides; Lattice defects; Vacancies; Non-destructive testing; Positron annihilation

1. Introduction

Good mechanical strength and excellent oxidation resistance at elevated temperatures make Fe–Al phases very attractive for high temperature applications [1,2]. It is well established that the physical and mechanical properties of Fe–Al alloys are strongly influenced by the atomic ordering and point defects [3]. It was shown that a high concentration of vacancies formed in Fe–Al alloys at high temperatures can be relatively easily quenched down to room temperature. The concentration of quenched-in vacancies increases with increasing Al content or quenching temperature and may be as high as several atomic percent [4–6]. It was convincingly demonstrated that the hardness and strength of Fe–Al alloys can be increased by vacancies [5,7]. Thus the investigation of vacancies is very important for understanding the physical properties of Fe–Al alloys. So far characterization of vacancies has been performed mostly in Fe–Al alloys with an Al content around Fe–Al stoichiometry, since these alloys exhibit the highest concentrations of vacancies. Less is know about vacancies in Fe–Al alloys with compositions close to the Fe_3Al stoichiometry.

During cooling from high temperatures Fe–Al alloys with an Al content in the range 22.7–40 at.% undergo ordering from the high temperature disordered A2 phase to the partially ordered B2 structure and subsequently to the ordered $D0_3$ phase [8,9]. The disordered high temperature phases can be retained in the samples by fast cooling. Structure of the Fe_3Al phases is based on two interpenetrating cubic sub-lattices, denoted A and B, which are shown in Fig. 1. In the disordered A2 phase both sub-lattices are randomly occupied by Fe and Al atoms. Hence, each lattice site in Fig. 1 is occupied by an Fe atom with probability 0.75 and by an Al atom with probability 0.25. In the partially ordered B2 phase the A sub-lattice is occupied exclusively by Fe atoms, while the B sub-lattice is randomly filled by Fe and Al. Thus, each site in the B sub-lattice is occupied by an Fe or Al atom with probability 0.5. The complex $D0_3$ phase is fully ordered, with the A sub-lattice occupied only by Fe atoms and the B sub-lattice consisting of alternating Fe and Al atoms (see Fig. 1).

* Corresponding author. Tel.: +420 221912788; fax: +420 221912567.
E-mail address: jakub.cizek@mff.cuni.cz (J. Čížek).

1359-6454/$36.00
doi:10.1016/j.actamat.2011.03.031

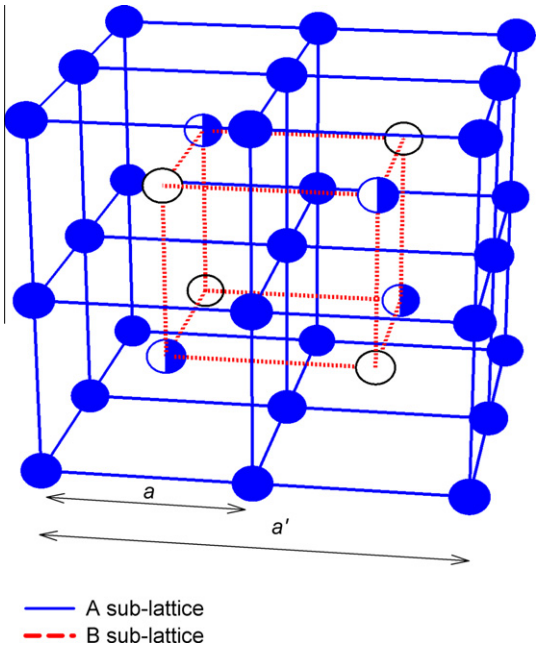

Fig. 1. The structure of the Fe_3Al phases. Solid and dashed lines show the A and B sub-lattices, respectively. In the disordered A2 phase the A and B sub-lattices are randomly occupied by Fe and Al atoms. In the partially ordered B2 phase the A sub-lattice is occupied exclusively by Fe atoms (full circles), while the B sub-lattice is filled randomly with Fe and Al atoms. The complex $D0_3$ structure consists of the A sub-lattice occupied only by Fe atoms (full circles) and the B sub-lattice consisting of alternating Fe (half filled circles) and Al (open circles) atoms. The symbol a denotes the lattice parameter of the A2 and B2 phases, while $a' = 2a$ is the lattice parameter of the complex $D0_3$ phase.

Positron annihilation spectroscopy (PAS) is a well-established, non-destructive technique with a high sensitivity to vacancies [10,11]. Moreover, positron characteristics can be calculated from first principles and directly compared with experiment [12]. PAS involves several experimental techniques. Among them, positron lifetime (LT) spectroscopy [10,11] and coincidence Doppler broadening (CDB) [13,14] are most suitable for the characterization of vacancies in Fe–Al alloys. LT spectroscopy enables the determination of the free volume and concentration of defects, while CDB provides information about the local chemical environment of defects.

LT spectroscopy has been employed to investigate vacancies in Fe–Al alloys by a number of authors [15–28]. In contrast, CDB studies of Fe–Al alloys are still rather rare [20,28], despite that fact that a knowledge of the chemical environment may significantly facilitate identification of vacancies. The lifetime of trapped positrons is to some extent influenced by the chemical environment of the vacancy. However, the dependence of the positron lifetime on chemical environment of a defect is relatively moderate. In Fe–Al alloys variations in the chemical environment of vacancies changes the lifetime of trapped positrons typically by a few picoseconds [16,28]. Hence, taking into account statistical scattering of the experimental data, unambiguous identification of vacancies is not always possible on the basis of LT results alone. This can be seen in Table 1, which summarizes the published lifetimes of positrons trapped in vacancies in Fe–Al alloys with compositions close to Fe_3Al. Positron lifetimes reported in the literature fall in the range 170–188 ps, with one exception of a rather short lifetime of 160 ps in Broska et al. [18]. From inspection of these data it is clear that additional information about the chemical environment of vacancies is highly desirable. The exceptional sensitivity of the CDB technique to elements in the vicinity of defects enables reconstruction of the chemical environment of vacancies. Hence, a combination of LT and CDB is an excellent method to investigate vacancies in Fe–Al alloys.

In this work we performed detailed investigations of thermal vacancies in stoichiometric Fe_3Al alloys employing LT spectroscopy combined with CDB. The phase composition of the samples was characterized by X-ray diffraction (XRD). The experimental PAS data were interpreted with the aid of ab inito theoretical calculations of the positron parameters.

2. Materials and methods

The stoichiometric Fe_3Al alloy was prepared from Fe (99.99% purity) and Al (99.99% purity) by induction co-melting under an Ar atmosphere. The Fe_3Al ingot was homogenized at 1000 °C and then cooled in a furnace. Samples for PAS investigations having the dimensions $10 \times 10 \times 1$ mm were cut from the Fe_3Al ingot. The samples were then encapsulated in evacuated silicon glass ampoules which were subsequently filled with argon and annealed at 1000 °C for 1 h. The annealing treatment was finished by quenching the ampoule in water at room temperature. Since the annealing treatment was performed in the region of the disordered A2 phase [8,9] it is expected that the A2 phase is retained in the quenched samples. After characterization of defects in the as-quenched alloy the specimens were isochronally annealed in steps of 40 °C for 40 min. Each annealing step was finished by quenching in oil and subsequent PAS investigations at room temperature.

A $^{22}Na_2CO_3$ positron source with an activity of 1.2 MBq deposited on a 2 μm thick Mylar foil was used for the LT and CDB studies. The source contribution consists of two components with lifetimes of ~368 ps and ~1.5 ns and intensities of ~8% and ~1%. These components represent the contribution of positrons annihilated in the source itself and in the covering foil.

A high resolution digital spectrometer [29,30] was employed for LT investigations of the alloys studied. The detector part of the digital LT spectrometer is equipped with two Hamamatsu H3378 photomultipliers coupled with BaF_2 scintillators. Detector pulses are sampled in real time by two ultra-fast Acqiris DC211 8 bit digitizers at a sampling frequency of 4 GHz. The digitized pulses are acquired by a PC and calculations carried out off-line by software using a new algorithm for integral constant

Table 1
Lifetimes τ_V of positrons trapped in vacancies in Fe–Al alloys with compositions close to Fe_3Al reported by various authors.

Alloy	τ_V (ps)	Thermal treatment applied	Reference
$Fe_{76.3}Al_{23.7}$	171 ± 1	In situ LT measurement	[15]
Fe_3Al	178	Water quenched from 1000 °C	[16]
Fe_3Al	188 ± 3	Air quenched from 1000 °C	[17]
Fe_3Al	182 ± 3	Slowly cooled from 1000 °C in furnace	[17]
Fe_3Al	181 ± 3	Air quenched from 1000 °C and aged at 520 °C for 1 week	[16]
Fe_3Al	160 ± 2	In situ LT measurement	[18]
Fe_3Al	182 ± 1	Water quenched from 1000 °C in an ampoule filled with Ar	This work
$Fe_{72}Al_{28}$	184 ± 1	Air quenched from 1000 °C	[19]
$Fe_{72}Al_{28}$	178	Oil quenched from 1000 °C	[20]
$Fe_{72}Al_{28}$	170 ± 2	Slowly cooled from 1000 °C	[21]

fraction timing [31]. The time resolution of the digital LT spectrometer was 150 ps (full width at half maximum (FWHM), ^{22}Na). At least 10^7 annihilation events were accumulated in each LT spectrum.

The CDB spectrometer consists of two HPGe detectors and commercial NIM modules operated by a PC. The overall energy resolution of the spectrometer was 1.0 keV (FWHM) at 511 keV energy. At least 10^8 events were collected in each two-dimensional spectrum, which was subsequently reduced to a one-dimensional Doppler profile and instrumental resolution cuts. The relative changes in Doppler profiles were followed as ratio curves of the Doppler profile normalized counts to those of a well-annealed α-Fe reference profile. The CDB profiles are symmetrical with respect to the origin and only the parts corresponding to positive Doppler shifts are shown here. Well-annealed pure α-Fe (99.99% purity) and Al (99.9999% purity) were used as reference specimens for the CDB measurements.

3. Theoretical calculations

Theoretical calculations of the positron lifetimes were performed within the so-called standard scheme employing the atomic superimposition (ATSUP) method [11,32,33]. The electron–positron correlations were treated according to Boroński and Nieminen [34].

The ATSUP-based scheme described in Kuriplach et al. [35] was utilized for calculations of high momentum parts (HMP) of the momentum distribution of annihilation photons. The electron–positron correlations were treated within the generalized gradient approximation (GGA) scheme introduced by Barbiellini et al. [36], which gives more accurate magnitudes of the contribution of positrons annihilated by core electrons. The calculated spectra were convoluted with a Gaussian function having a width of $4.0 \times 10^{-3}\ m_e c$ (FWHM), which corresponds to the experimental energy resolution of our CDB spectrometer. In HMP calculations [Ne] orbitals were considered as core states for Al and $[Ar] + 3d^6$ ones for Fe. The contribution of Fe 3d electrons was weighted by a factor of 0.5 to account for the semi-core character of d orbitals. It was found that this approach gives the best agreement of the HMP of momentum distribution calculated for Fe with the experimental results [37]. The lattice parameter used in calculations was $a = 2.896$ Å [38]. Calculations for vacancies were performed using a supercell approach, considering 1024 atom-based supercells. Monovacancies were created by removing single atoms from the supercell. The disordered A2 and partially disordered B2 structures were modeled by random filling of the atomic positions in both sub-lattices and in the B sub-lattice, respectively, keeping the Fe_3Al composition in the supercell.

4. Results and discussion

4.1. LT spectroscopy

The as-quenched Fe_3Al alloy exhibits a two component LT spectrum consisting of: (i) a short-lived component with lifetime $\tau_1 = 27 \pm 9$ ps and relative intensity $I_1 = 10 \pm 1\%$, which arises from free positrons not trapped at defects, and (ii) a longer component with lifetime $\tau_2 = 182 \pm 1$ ps and relative intensity $I_2 = 90 \pm 1\%$, which represents the contribution of positrons trapped in quenched-in vacancies. One can see in Table 1 that the lifetime τ_2 determined in the as-quenched sample falls in the interval 170–188 ps, which covers lifetimes reported in literature for positrons trapped in vacancies in Fe–Al alloys with composition close to Fe_3Al.

Lifetimes τ_1 and τ_2 are plotted in Fig. 2A as a function of the annealing temperature, while Fig. 2B shows the temperature dependence of the relative intensity I_2 of the component corresponding to positrons trapped in vacancies. The lifetime τ_2 remains approximately constant during annealing, indicating that the type of positron trap remains unchanged. The intensity I_2 strongly decreases after annealing above 400 °C and reaches a minimum at ~480 °C. This proves substantial recovery of quenched-in vacancies. Further annealing above 500 °C leads to a pronounced increase in I_2. This indicates that the concentration of vacancies in the sample increases again.

4.2. Concentration of vacancies

The concentration of vacancies was determined using the two state simple trapping model (STM) [11,39]. Firstly it is necessary to check whether STM assumptions, namely the existence of a single type of uniformly distributed positron trap and no detrapping, are fulfilled in the samples studied. The quantity τ_f calculated from expression

$$\tau_f = \left(\frac{I_1}{\tau_1} + \frac{I_2}{\tau_2}\right)^{-1} \quad (1)$$

is plotted in Fig. 2A. Within STM [11,39] τ_f equals the bulk positron lifetime τ_B, i.e. the lifetime of free positrons in a perfect Fe_3Al crystal. From inspection of Fig. 2A it is clear

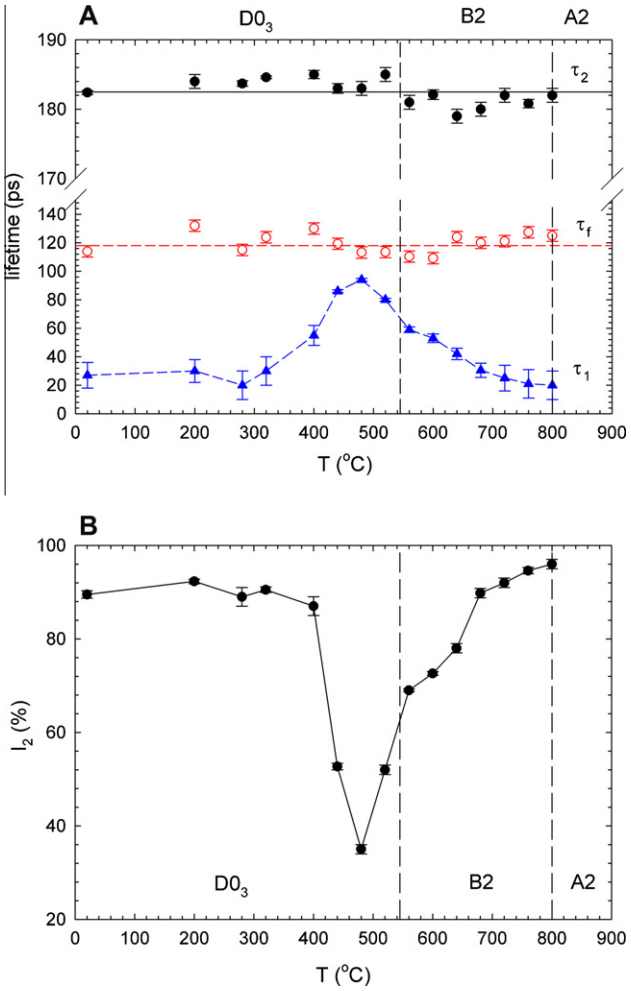

Fig. 2. The results of LT investigations plotted as a function of the annealing temperature. (A) Lifetimes τ_1, τ_2 of the exponential components resolved in the LT spectra and the quantity τ_f calculated from Eq. (1). (B) Intensity I_2 of the component originating from positrons trapped in vacancies. The vertical dashed lines show the positions of phase boundaries between the $D0_3$, B2 and A2 phases.

that τ_f remains approximately constant over the whole temperature range and exhibits only statistical fluctuations around the mean value of 118 ± 5 ps, which is comparable with the bulk positron lifetime $\tau_B = 112$ ps measured in a well-annealed Fe_3Al [15,19]. This proves that STM assumptions are fulfilled here and STM can be applied to determine the vacancy concentration.

The concentration of vacancies in the sample can be calculated from the expression

$$c_V = \frac{1}{\nu_V} I_2 \left(\frac{1}{\tau_1} - \frac{1}{\tau_2} \right) \quad (2)$$

where the symbol ν_v denotes the specific positron trapping rate in vacancies. Here we used $\nu_v = 4 \times 10^{14}\ s^{-1}$, determined for vacancies in an Fe_3Al alloy in Schaefer et al. [15]. The concentration of vacancies calculated from Eq. (2) is plotted in Fig. 3 as a function of the annealing temperature. The vertical lines in Fig. 3 show the positions of phase boundaries between various phases in the equilibrium phase diagram [8,9]. The Fe_3Al sample was initially annealed at 1000 °C, i.e. in the region corresponding to the disordered A2 phase. Due to the high cooling rate the disordered A2 structure is retained in the as-quenched sample. Hence, it is expected that the as-quenched sample contains mostly A2 phase. This assumption was confirmed by the XRD pattern determined for the as-quenched sample, which is plotted in Fig. 4, and contains only reflections corresponding to the disordered A2 phase. The lattice parameter $a = 2.918 \pm 0.004$ Å obtained from fitting of the XRD pattern is in reasonable agreement with that determined in the disordered A2 phase of Fe_3Al in Taylor and Jines [40].

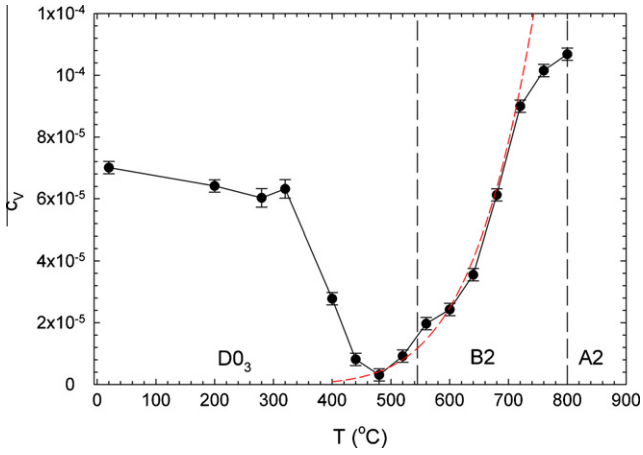

Fig. 3. Temperature dependence of the concentration of vacancies c_V determined from the LT results using Eq. (2). The vertical dashed lines show the positions of phase boundaries between the $D0_3$, B2 and A2 phases. The dashed curve is the equilibrium concentration of vacancies calculated using Eq. (3) with $H_{V,f} = 0.84$ eV and $S_{V,f} = 0.6\ k$.

Hence, although the existence of small domains of partially ordered B2 phase cannot be excluded [41], we can conclude that the as-quenched sample contains predominantly the disordered A2 phase. One can see in Fig. 3 that the concentration of vacancies in the as-quenched sample is $c_V \approx 7 \times 10^{-5}$ and remains almost unchanged during subsequent annealing up to ~350 °C. Above this temperature c_V strongly decreases and a minimum vacancy concentration is reached at ~480 °C. This behavior indicates that vacancies in Fe_3Al become mobile above 350 °C and disappear by diffusion into sinks. Ordering of the disordered as-quenched structure into $D0_3$ phase takes place simultaneously with the recovery of vacancies. This is confirmed by the XRD results shown in Fig. 4. From an inspection of the XRD pattern measured in the sample annealed at 480 °C one can conclude the following:

i. Superstructure reflections (1 1 1) and (2 0 0) corresponding to the $D0_3$ phase appeared in the XRD pattern annealed at 480 °C.
ii. There is a significant narrowing of the XRD reflections in comparison with the as-quenched sample. This indicates that variations in the inter-atomic spacing caused by atomic disorder diminished in the sample annealed at 480 °C.

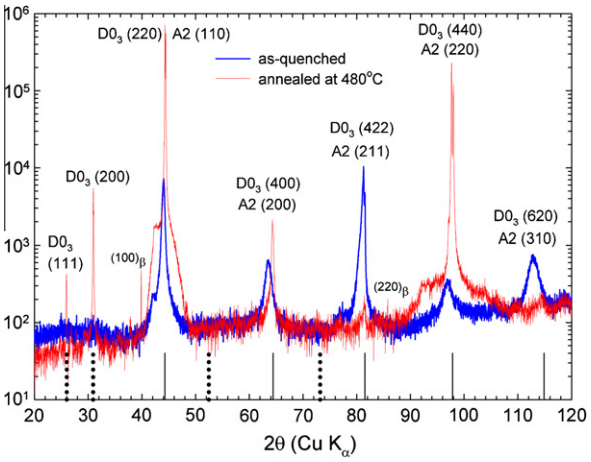

Fig. 4. XRD diffraction pattern measured on the as-quenched alloy and the sample annealed up to 480 °C. Indices for detected reflections corresponding to the disordered A2 phase and the ordered $D0_3$ phase are shown in the figure. Weak reflections from Cu K_β X-rays visible in the spectrum are also labeled with the subscript β. Calculated positions of reflections for both phases are indicated by vertical lines at the bottom. Solid lines show reflections common for the A2 and $D0_3$ phases. Positions of superstructure reflections which can be seen only in the ordered $D0_3$ phase are indicated by dotted vertical lines.

iii. The lattice parameter in the sample annealed at 480 °C was lower compared with the as-quenched alloy, which is shown by a shift of the XRD reflections to larger diffraction angles (see Fig. 4). A decrease in the lattice parameter is caused by atomic ordering into the $D0_3$ structure [42].

Hence, all these findings prove atomic ordering and formation of the $D0_3$ structure in the sample annealed at 480 °C. The $D0_3$ phase lattice parameter $a' = 2a = 5.799 \pm 0.002$ Å was obtained from fitting the XRD pattern. Note that because of a more complex structure the lattice parameter a' corresponding to the $D0_3$ basic cubic cell is twice that of the B2 and A2 structures (see Fig. 1).

4.3. Vacancy formation enthalpy

The equilibrium concentration of vacancies at temperature T is governed by the expression

$$c_V = \exp\left(\frac{S_{V,f}}{k}\right)\exp\left(-\frac{H_{V,f}}{kT}\right) \quad (3)$$

where k is the Boltzman constant and the symbols $H_{V,f}$ and $S_{V,f}$ denote the enthalpy and entropy of vacancy formation, respectively. At temperatures above 500 °C the concentration of thermal vacancies becomes high enough ($c_V \geqslant 10^{-5}$) to be detected by PAS. Thermal vacancies created during each annealing step at temperature T remain frozen in the sample due to rapid cooling and cause a substantial increase in c_V above 500 °C, which can be seen in Fig. 3. Note that at $T > 700$ °C the vacancy concentration exceeds that even in the as-quenched sample. This is due to the faster cooling rate, since isochronally annealed samples are quenched in an oil bath, i.e. they are in direct contact with the cooling liquid. This leads to a faster cooling rate compared with the initial sample, which was quenched in an ampoule filled with argon.

Atom disordering in the B sub-lattice takes place in the sample annealed above 545 °C when the phase boundary between the ordered $D0_3$ and the partially ordered B2 phase is crossed. In the temperature interval 545–800 °C the sample exhibits B2 structure [8,9]. Therefore, thermal vacancies detected by PAS are formed mainly in the B2 structure.

Hence, the temperature dependence of vacancy concentration plotted in Fig. 3 can be used to determine the enthalpy $H_{V,f}$ and entropy $S_{V,f}$ of vacancy formation in the B2 phase. Fig. 5 shows an Arrhenius plot ($\ln c_V$ versus $1/kT$) constructed using vacancy concentrations detected at temperatures $T > 500$ °C, where thermal vacancies become detectable by PAS. One can see in Fig. 5 that the Arrhenius plot can be reasonably approximated by a straight line up to $T \approx 700$ °C. At higher temperatures the loss of vacancies during cooling becomes significant and the concentration of quenched-in vacancies is smaller than predicted by Eq. (3). This is reflected in a significantly lowered slope in the Arrhenius plot. Due to this the determination of $H_{V,f}$ and $S_{V,f}$ from the Arrhenius plot was performed by linear regression only in the temperature range 500–700 °C (see the solid line in Fig. 5). The enthalpy of vacancy formation obtained from the Arrhenius plot $H_{v,f} = 0.84 \pm 0.05$ eV falls in the range 0.73–1.18 eV reported in the literature for vacancies in the B2 phase. The entropy of vacancy formation obtained from the Arrhenius plot is $S_{v,f} = 0.6 \pm 0.4k$.

To put the enthalpy of formation derived here in the context of results published in the literature, Fig. 6 shows $H_{V,f}$ values for vacancies in the B2 phase in Fe–Al alloys

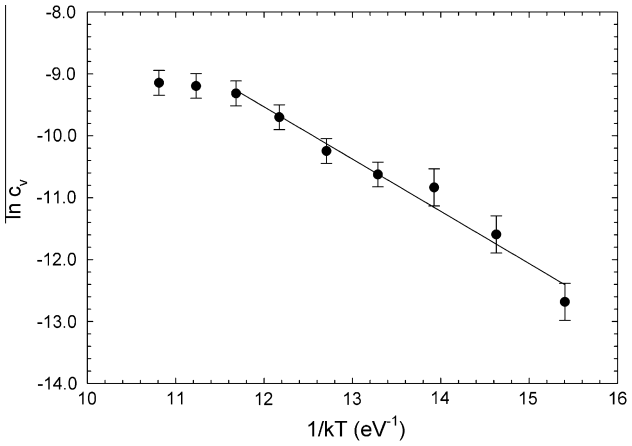

Fig. 5. Arrhenius plot constructed from the vacancy concentrations determined by LT spectroscopy in the sample subjected to isochronal annealing at temperatures $T \geqslant 500$ °C. Solid line shows linear regression of the data in the temperature range 500–700 °C.

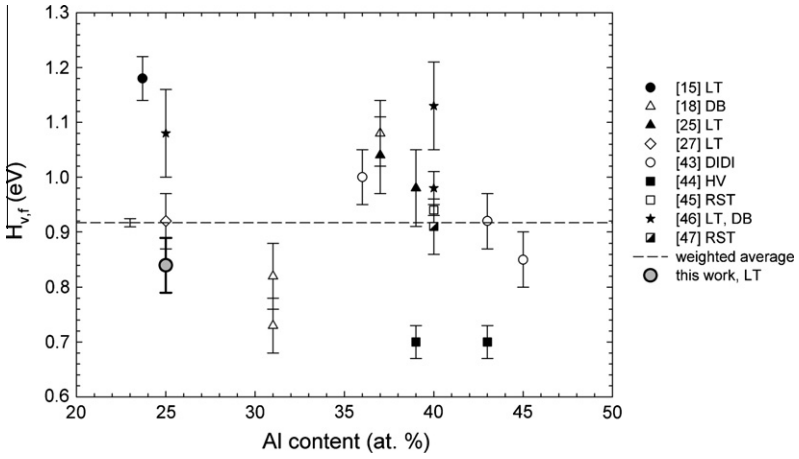

Fig. 6. The vacancy formation enthalpy $H_{V,f}$ for vacancies in the B2 phase reported for Fe–Al alloys by various authors. The data are plotted as a function of Al content. The dashed line is the weighted average calculated from of all data taking into account the uncertainty of each quantity. Abbreviations in the legend denote the experimental technique employed for determination of $H_{V,f}$. LT, positron lifetime spectroscopy; DB, Doppler broadening of annihilation radiation; DIDI, differential dilatomery; HV, hardness measurement; RST, resistometry.

with various compositions published in the literature [15,18,25,27,43–47]. One can see in Fig. 5 that $H_{V,f}$ is basically independent of the Al content. The weighted average calculated from the literature data taking into account the uncertainty of each quantity is $H_{v,f} = 0.917 \pm 0.008$ eV, which is in reasonable agreement with the enthalpy of formation obtained in this work.

There is a lack of information about the entropy of vacancy formation in the B2 phase. However, it should be mentioned that our value is significantly lower than $S_{v,f} \approx 5k$ determined in Lynn et al. [13] for vacancies in the $D0_3$ phase.

4.4. CDB spectroscopy

The CDB results are plotted in Fig. 7 as ratio curves related to the pure Fe reference specimen. The ratio curve for a pure Al reference specimen is also plotted in the figure. The main feature of the pure Al CDB curve is a broad minimum in the momentum range $p \approx (10–20) \times 10^{-3} m_0 c$. This is caused mainly by the absence of 3d electrons in Al. The shape of the CDB curve for the as-quenched Fe_3Al sample exhibits the same features as the curve for pure Al. This indicates that a significant fraction of positrons in the as-quenched Fe_3Al sample is annihilated by Al electrons. Since core electrons are only slightly affected by crystal bonding and retain their atomic character, the HMP of the momentum distribution in the Fe_3Al alloy can be expressed as the linear combination

$$n = \xi_{Al} n_{Al} + (1 - \xi_{Al}) n_{Fe} \quad (4)$$

where n_{Al} and n_{Fe} are the momentum distribution of positrons annihilated by Al and Fe electrons, respectively, and ξ_{Al} is the fraction of positrons annihilated by Al electrons. Hence, the CDB ratio curve $\rho = n/n_{Fe}$ in an Fe_3Al alloy is

$$\rho = \xi_{Al} \rho_{Al} + (1 - \xi_{Al}) \quad (5)$$

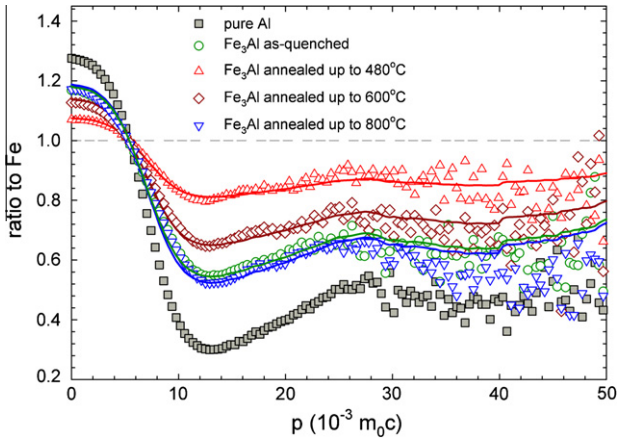

Fig. 7. Selected CDB ratio curves (related to pure Fe) for the as-quenched Fe_3Al and the samples annealed at 480, 600 and 800 °C. The ratio curve for pure Al is plotted as well. Solid lines show best fits using Eq. (5).

Here $\rho_{Al} = n_{Al}/n_{Fe}$ is the CDB ratio curve for pure Al. The solid curves in Fig. 7 show the CDB ratio curve ρ_{Al} for pure Al rescaled using Eq. (5). Obviously, the CDB ratio curve measured on the as-quenched sample is well approximated by Eq. (5). The best agreement with the experimental points was obtained for the fraction of positrons annihilated by Al electrons $\xi_{Al} = 0.65 \pm 0.02$.

The CDB ratio curves measured on the samples subjected to isochronal annealing are plotted in Fig. 7 as well. For the sake of clarity only selected CDB curves measured on the sample annealed up to 480, 600 and 800 °C are plotted in Fig. 7. All CDB ratio curves measured on isochronaly annealed samples are shown as a two-dimensional plot in Fig. 8. No significant changes in CDB curves were observed up to ~350 °C. At higher temperatures the contribution of positrons annihilated by Al electrons decreases and the CDB ratio curves become closer to a straight horizontal line, i.e. unity, representing the curve for pure Fe.

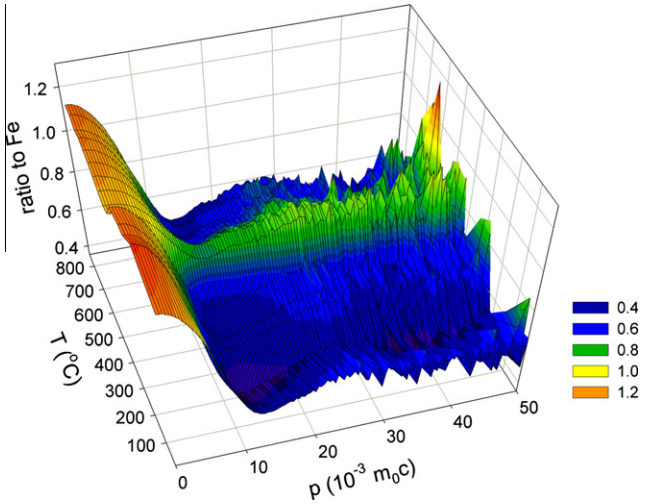

Fig. 8. Two-dimensional plot of CDB ratio curves (related to Fe) for Fe_3Al samples annealed at various temperatures.

The smallest contribution of positrons annihilated by Al electrons was found in the sample annealed at 480 °C (see also Fig. 7). Further annealing to higher temperatures causes an increase in the fraction of positrons annihilated by Al electrons.

It should be mentioned that all CDB ratio curves measured on isochronaly annealed samples are satisfactorily approximated by Eq. (5). The fraction of positrons annihilated by Al electrons obtained by fitting to Eq. (5) is plotted in Fig. 9 as a function of the annealing temperature. One can see in Fig. 9 that ξ_{Al} remains almost unchanged up to to ~350 °C where it strongly decreases and reaches its minimum at ~480 °C. Annealing to higher temperatures causes a significant increase in ξ_{Al}.

Positrons in Fe_3Al alloys annihilate either from the free state or from the trapped state in a vacancy. The probability of being annihilated by Al electrons differs in these two states. Hence, Eq. (4) can be rewritten using the contributions of positrons annihilated from the free state and from the trapped state in vacancies

$$n = (1 - F_V)[\xi_{Al,B} n_{Al} + (1 - \xi_{Al,B}) n_{Fe}] + F_V[\xi_{Al,V} n_{Al} + (1 - \xi_{Al,V}) n_{Fe}] \quad (6)$$

where $\xi_{Al,B}$ and $\xi_{Al,V}$ denote the probability that a positron in the free state and in the trapped state in a vacancy, respectively, will be annihilated by an Al electron. The symbol F_V denotes the fraction of positrons annihilated from the trapped state in vacancies. The CDB ratio curve ρ can be then be written as

$$\rho = [(1 - F_V)\xi_{Al,B} + F_V \xi_{Al,V}]\rho_{Al} + [(1 - F_V) \times (1 - \xi_{Al,B}) + F_V(1 - \xi_{Al,V})] \quad (7)$$

The fraction F_V can be calculated from the LT data using STM [11]

$$F_V = I_2\left(1 - \frac{\tau_1}{\tau_2}\right) \quad (8)$$

The dependence of F_V on the annealing temperature is plotted in Fig. 9. Obviously the behaviors of F_V and ξ_{Al} are very similar. Thus, the recovery of vacancies starting at 350 °C is accomplished by a decrease in the fraction of positrons annihilated by Al electrons. Similarly, the increase in the concentration of vacancies which occurs above 500 °C is accompanied by an increase in the fraction of positrons annihilated by Al electrons.

From comparison of Eqs. (5) and (7) one obtains expression

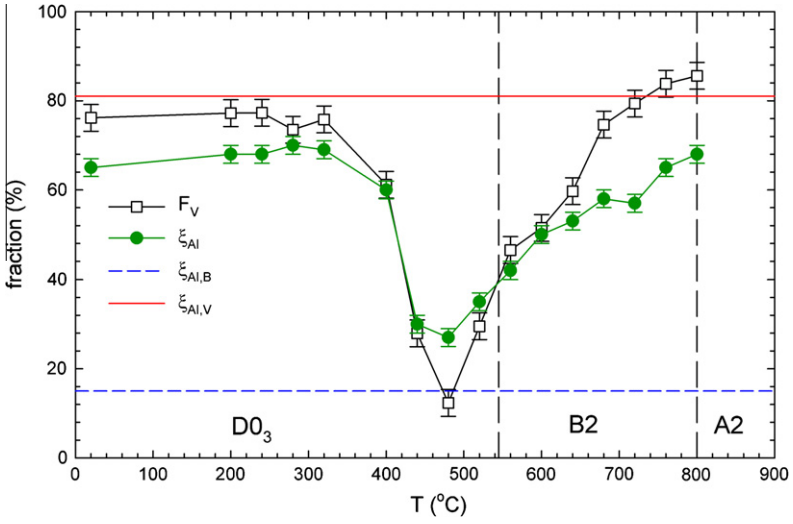

Fig. 9. Temperature dependence of the fraction of positrons annihilated by Al electrons ξ_{Al} obtained by fitting CDB curves using Eq. (5), plotted as filled circles and the fraction F_V of positrons trapped in vacancies calculated from the LT data using Eq. (8), plotted as open symbols. The vertical dashed line shows the probability $\xi_{Al,B}$ that a free positron is annihilated by an Al electron. The vertical solid line shows the probability $\xi_{Al,V}$ that a positron trapped in a vacancy is annihilated by an Al electron.

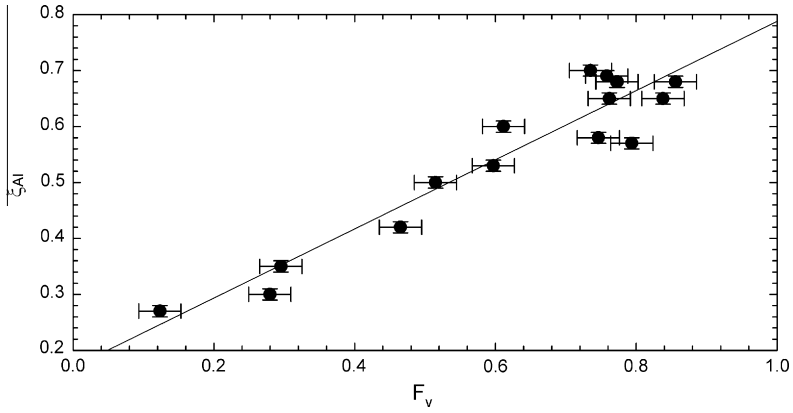

Fig. 10. The fraction of positrons annihilated by Al electrons obtained from fitting CDB curves using Eq. (5) plotted versus the fraction F_V of positrons trapped in vacancies calculated from the LT data using Eq. (8). The solid line is the linear regression curve used to determine the probabilities $\xi_{Al,B}$ and $\xi_{Al,V}$ (see Eq. (9)).

$$\xi_{Al} = (\xi_{Al,V} - \xi_{Al,B})F_V + \xi_{Al,B} \quad (9)$$

Hence, there is a linear relation between the fraction ξ_{Al} of positrons annihilated by Al electrons and the fraction F_V of positrons trapped in vacancies. Indeed, one can see in Fig. 10 that the dependence of ξ_{Al} on F_V can be reasonably approximated by a straight line. Linear regression of the data in Fig. 10 yields $\xi_{Al,B} = 0.17 \pm 0.01$ and $\xi_{Al,V} = 0.79 \pm 0.01$. From ab initio theoretical calculations of positrons in a perfect Fe_3Al crystal with B2 structure we obtained the probability that a free positron is annihilated by an Al electron $\xi_{Al,B} = 0.15$, which is in very reasonable agreement with the value obtained from fitting the experimental data. A similar value was obtained for the $D0_3$ and A2 phases. Note that scattering of the calculated $\xi_{Al,B}$ values caused by random filling of the sites in the B sub-lattice by Fe and Al atoms (always keeping the total composition equal to Fe_3Al) was found to be negligible. The value of $\xi_{Al,V}$ derived from the experimental data indicates that for positrons trapped in vacancies the probability of being annihilated by Al electrons is rather high. This indicates that quenched-in vacancies are predominantly surrounded by Al atoms. This is not surprising, since Al atoms, having a larger "size" in the lattice, should be attracted to the vicinity of a vacancy.

4.5. Theoretical calculations

Numerous theoretical investigations [48–51] performed for the B2 phase came to the general conclusion that the enthalpy of vacancy formation in the B sub-lattice is significantly higher than in the A sub-lattice. Thus, thermal vacancies in the B2 phase should be Fe vacancies (V_{Fe}) located in the A sub-lattice. In the B2 phase V_{Fe} in the A sub-lattice is surrounded by eight nearest neighbors located in the B sub-lattice and six next nearest neighbors in the A sub-lattice (see Fig. 1). While the next nearest neighbors in the A sub-lattice are always Fe, the nearest neighbor sites in the B sub-lattice may be occupied by Fe or Al atoms.

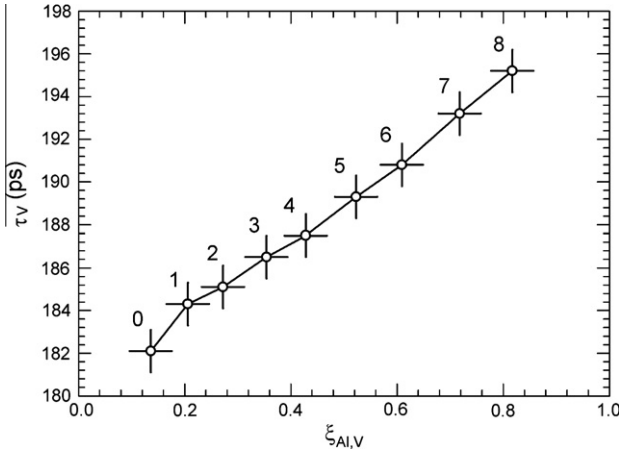

Fig. 11. Calculated lifetime of positrons trapped in V_{Fe} plotted versus the calculated probability $\xi_{Al,V}$ that a trapped positron will be annihilated by an Al electron. Labels in the figure show the number of vacancy nearest neighbors occupied by Al atoms. Bars around each point represent the magnitude of scattering of the calculated parameters due to random filling of vacancy higher order neighbors by Fe and Al atoms.

Fig. 11 shows the calculated lifetime τ_V of positrons trapped in a V_{Fe} plotted against the calculated probability $\xi_{Al,V}$ that a trapped positron will be annihilated by an Al electron. The labels in the figure show the number NN_{Al} of nearest neighbor sites occupied by Al atoms ($0 \leqslant NN_{Al} \leqslant 8$), i.e. the remaining 8-$NN_{Al}$ nearest neighbor sites are occupied by Fe atoms. Note that other than nearest neighbor sites in the B sub-lattice were randomly filled with Fe and Al atoms, keeping the total composition in the supercell equal to Fe_3Al. Fluctuations in the type of atoms in higher order neighbors of V_{Fe} cause scattering of the calculated positron parameters, indicated by bars around the points in Fig. 11. The lifetime of positrons trapped in V_{Fe} clearly increases with increasing number of the nearest sites occupied by Al atoms. A comparison of the theoretical calculations with the experimental results makes clear that the experimental lifetime of positrons trapped in quenched-in

vacancies $\tau_2 \approx 182$ ps is comparable with the lifetime calculated for V_{Fe} surrounded only by Fe atoms in the nearest neighbor sites ($NN_{Al} = 0$). On the other hand, the probability that a trapped positron is annihilated by an Al electron determined from the CDB data $\xi_{Al,V} \approx 0.79$ corresponds roughly to a V_{Fe} surrounded exclusively by Al nearest neighbors ($NN_{Al} = 8$). However, the latter defect is characterized by a positron lifetime of 195 ps, which is significantly longer than τ_2. This discrepancy is probably due to the limited precision of the ATSUP approach, which does not take into account: (i) charge transfer in the crystal and (ii) lattice relaxations around the vacancy. Calculations performed by Ishida et al. [52] showed a strong charge transfer from Al to Fe. This effect may enhance the local electron density in V_{Fe}. Inward relaxation of the nearest neighbor Al atoms towards a V_{Fe} reduces the free volume in the vacancy. The effect of ion relaxation on the lifetime of positrons trapped in a V_{Fe} surrounded by eight Al nearest neighbors is depicted in Fig. 12, which shows the dependence of positron lifetime on the magnitude of inward relaxation of the nearest neighbor Al atoms. One can see in the figure that a relaxation of ~3% results in the calculated lifetime for positrons trapped in a V_{Fe} surrounded by eight Al nearest neighbors being comparable with the experimental value $\tau_2 \approx 182$ ps. Hence, both factors (i) and (ii) cause a shortening of the positron lifetime and may reduce the lifetime of positrons trapped in a V_{Fe} surrounded by eight Al nearest neighbors to the value measured in the experiments. Obviously, extended theoretical calculations of positron parameters using a self-consistent electron density and a relaxed geometry of defects are highly desirable in order to verify the picture suggested here.

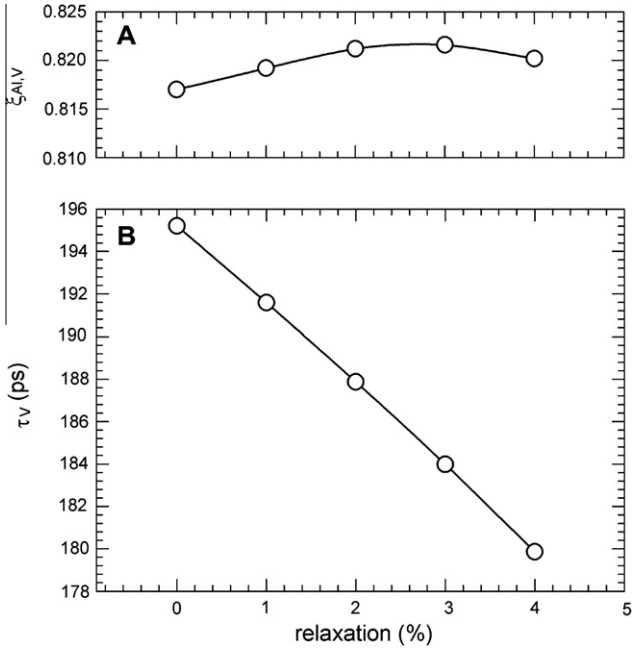

Fig. 12. The effect of the lattice relaxation around a V_{Fe} surrounded by eight nearest neighbor Al atoms: dependence of the calculated positron parameters on the magnitude of inward relaxation of nearest neighbors. (A) The probability that a positron trapped in a V_{Fe} is annihilated by an Al electron. (B) Lifetime of positrons trapped in a V_{Fe}.

Fig. 13A shows calculated HMP for the momentum distribution of annihilation radiation (related to pure Fe) for a perfect Fe_3Al crystal and a V_{Fe} with no, four and eight Al atoms in the nearest neighbor sites. Since our calculations were performed only for core electrons, it is meaningful to compare the calculated curves with the experimental ones only in the HMP range ($p > 10 \times 10^{-3} m_0 c$) when the contribution of core electrons dominates. Clearly, the curves for vacancies are located well below that for a perfect crystal. This is due to positron localization in vacancies, which reduces the overlap with core electrons. A V_{Fe} surrounded only by Fe atoms in the nearest neighbor sites ($NN_{Al} = 0$) exhibits rather flat HMP of the momentum distribution curve. A broad minimum in the momentum range $p \approx (10–20) \times 10^{-3} m_0 c$ observed in

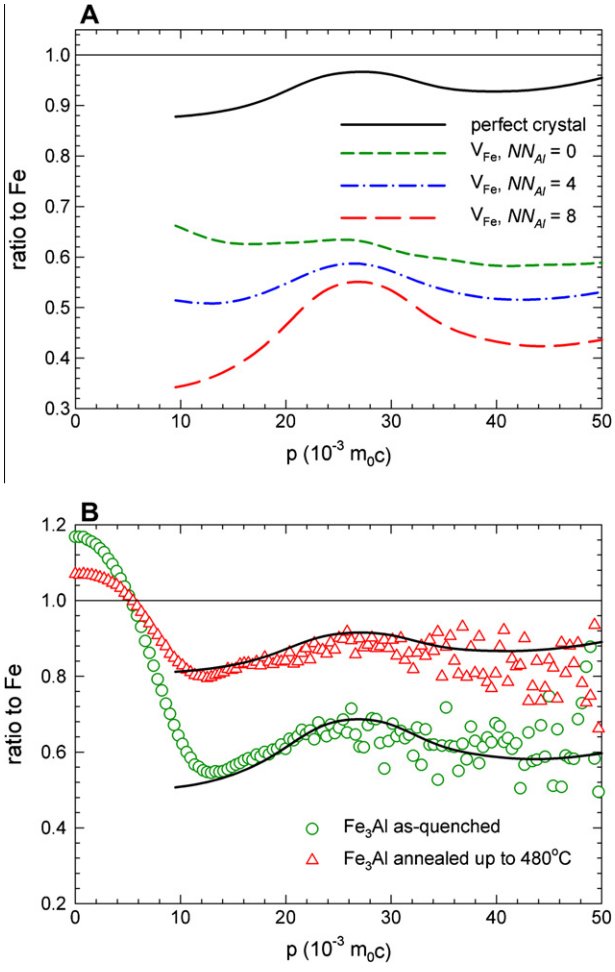

Fig. 13. (A) The calculated HMP of the momentum distribution of annihilation radiation for free positrons in perfect Fe_3Al crystals and for positrons trapped in a V_{Fe} with no, four and eight nearest neighbor sites occupied by Al. (B) Comparison of the HMP of the momentum distribution calculated using Eq. (10) (plotted as solid lines) with experimental CDB curves measured on the as-quenched alloy and the sample annealed at 480 °C.

the experimental CDB curves (see Fig. 7) is well reproduced in the calculated curves for a V_{Fe} with Al nearest neighbors. This minimum becomes more pronounced with increasing number of Al atoms occupying the nearest neighbor sites (see Fig. 13A). The momentum distribution in the sample annealed at temperature T is a linear combination of the contribution of positrons annihilating in the free state and the contribution of positrons trapped in vacancies. Hence, the CDB ratio curve is

$$\rho = [1 - F_V(T)]\rho_B + F_V(T)\rho_{V_{Fe}} \quad (10)$$

where ρ_B and $\rho_{V_{Fe}}$ denote the calculated HMP of the momentum distribution for a perfect Fe_3Al crystal and a V_{Fe} surrounded by eight Al nearest neighbors ($NN_{Al} = 8$), respectively, and $F_V(T)$ is the fraction of positrons trapped in vacancies at a given temperature calculated using Eq. (8). One can see in Fig. 13A that the HMP of the momentum distribution calculated using Eq. (10) are in very reasonable agreement with the experimental CDB curves. A similar agreement with the experimental results was achieved at other annealing temperatures. It should be emphasized that there is no adjustment parameter in Eq. (10). Good agreement between the theoretical calculations and the experimental results supports our interpretation of the experimental data.

5. Conclusions

Vacancies in Fe_3Al alloys were investigated using LT spectroscopy combined with CDB measurements. The sample quenched from 1000 °C predominantly exhibits the disordered A2 structure. The concentration of vacancies in this sample is 7×10^{-5}. It was found that recovery of quenched-in vacancies starts at ~350 °C and is accompanied by atomic ordering to the $D0_3$ phase. The lowest concentration of vacancies was found in the sample annealed at 480 °C. In the sample annealed above 500 °C the equilibrium concentration of thermal vacancies becomes high enough to be detected and the sample undergoes phase transition into the partially ordered B2 phase. The enthalpy of formation $H_{v,f} = 0.84 \pm 0.05$ eV of vacancies in the B2 phase was determined from the LT results. The CDB investigations revealed that vacancies in the B2 phase are predominantly surrounded by Al atoms. The fraction of positrons annihilated by Al electrons was proved to be directly related to the fraction of positrons trapped in vacancies. From a comparison of the experimental data with the available theoretical calculations it is suggested that thermal vacancies in the B2 phase are Fe vacancies located in the A-sublattice surrounded by eight nearest neighbor Al atoms in the B-sublattice. Hence, our results indicate an attractive interaction between Al atoms and Fe vacancies. Theoretical calculations showed that the lifetime of positrons trapped in vacancies increases with increasing number of nearest neighbor sites occupied by Al atoms. Good agreement of the calculated HMP of momentum distribution with the experimental CDB curves was achieved.

Acknowledgments

The authors are grateful to J. Kuriplach (Charles University in Prague) for providing them with the ATSUP code. This work was supported by the Czech Scientific Foundation (Projects No. p108/11/1350 and No. GA106/08/P133), The Academy of Science of the Czech Republic (Project No. KAN300100801) and by the Ministry of Education, Youth and Sports of the Czech Republic through Research Plan No. MSM 0021620834.

References

[1] Sautho G. Intermetallics. Weinheim, Germany: VCH; 1995.
[2] Westbrook JH, Fleischer RL. Intermetallic compounds – principles and practice, vols. 1 and 2. Chichester: Wiley; 1994.
[3] Jordan JL, Derbi SC. Intermetallics 2003;11:507.
[4] Ho K, Dodd RA. Scr Metall 1978;12:1055.
[5] Chang YA, Pike LM, Liu CT, Bilbrey AR, Stone DS. Intermetallics 1993;1:107.
[6] Krachler R, Ipser H, Sepiol B, Vogl G. Intermetallics 1995;3:83.
[7] Yang Y, Baker I. Intermetallics 1998;6:167.
[8] Kubaschewski O. Iron-binary phase diagrams. Berlin: Springer; 1982. p. 5.
[9] Massalski TB. Binary alloy phase diagrams. Metals Park, OH: ASM; 1986.
[10] Hautojärvi P. Positrons in solids. Berlin: Springer-Verlag; 1979.
[11] Hautojärvi P, Corbel C. In: Dupasquier A, Mills AP, editors. Positron spectroscopy of solids. Proceedings of the international school of physics "Enrico Fermi". Amsterdam: IOS Press; 1995. p. 491.
[12] Puska MJ, Nieminen RM. Rev Mod Phys 1994;66:841.
[13] Lynn KG, MacDonald JR, Boie RA, Feldman LC, Gabbe JD, Robbins MF, et al. Phys Rev Lett 1977;38:241.
[14] Asoka-Kumar P, Alatalo M, Ghosh VJ, Kruseman AC, Nielsen B, Lynn KG. Phys Rev Lett 1996;77:2097.
[15] Schaefer HE, Würschum R, Šob M, Žák T, Yu WZ, Eckert W, et al. Phys Rev B 1990;41:11869.
[16] de Diego N, Plazaola F, Jiménez JA, Serna J, del Río J. Acta Mater 2005;53:163.
[17] Ortega Y, de Diego N, Plazaola F, Jiménez JA, del Ríoe J. Intermetallics 2007;15:177.
[18] Broska A, Wolff J, Franz M, Hehenkamp Th. Intermetallics 1999;7:259.
[19] Jirásková Y, Schneeweiss O, Šob M, Novotný I. Acta Mater 1997;45:2147.
[20] Somieski B, Schneibel JH, Hulett LD. Philos Mag Lett 1999;79:115.
[21] Kansy J, Hanc A, Giebel D, Jabllońska M. Acta Phys Polon A 2008;113:1409.
[22] Schaefer HE, Damson B, Weller M, Arzt E, George EP. Phys Stat Solid A 1997;160:531.
[23] Jirásková Y, Schneeweiss O, Šob M, Novotný I, Procházka I, Bečvář F, et al. J Phys 1995;5:C1.
[24] Gialanella S, Brusa RS, Deng W, Marino F, Spataru T, Principi G. J Alloys Compd 2001;317–318:485.
[25] Würschum R, Grupp C, Schaefer HE. Phys Rev Lett 1995;75:97.
[26] Haraguchi T, Hori F, Oshima R, Kogachi M. Intermetallics 2001;9:763.
[27] Wolff J, Franz M, Hehenkamp Th. J Radioanal Nucl Chem 1996;210:591.

[28] Melikhova O, Čížek J, Procházka I, Kuriplach J, Lukáč F, Cieslar M, et al. Phys Stat Solid C 2009;6:2367.
[29] Bečvář F, Čížek J, Procházka I, Janotová J. Nucl Instrum Methods A 2005;539:372.
[30] Bečvář F, Čížek J, Procházka I. Acta Phys Polon A 2008;113:1279.
[31] Bečvář F. Nucl Instrum Methods B 2007;261:871.
[32] Puska MJ, Nieminen RM. J Phys F 1983;13:333.
[33] Seitsonen AP, Puska MJ, Nieminen RM. Phys Rev B 1995;51:14057.
[34] Boroński E, Nieminen RM. Phys Rev B 1986;34:3820.
[35] Kuriplach J, Morales AL, Dauwe C, Segers D, Šob M. Phys Rev B 1998;58:107475.
[36] Barbiellini B, Puska MJ, Torsti T, Nieminen RM. Phys Rev B 1995;51:7341.
[37] Čížek J, Vlček M, Procházka I. Nucl Instrum Methods A 2010;623:982.
[38] Wakiyama T. J Phys Soc Jpn 1972;32:1222.
[39] West R. In: Hautojärvi P, editor. Positrons in solids. Berlin: Springer-Verlag; 1979. p. 89.
[40] Taylor A, Jines RM. J Phys Chem Solids 1958;6:16.
[41] Warlinomt H. Z Matallkde 1969;60:195.
[42] Negri D, Yavari AR, Deriu A. Acta Mater 1999;47:4545.
[43] Kerl R, Wolff J, Hehenkamp Th. Intermetallics 1999;7:301.
[44] Morris MA, George O, Morris DG. Mater Sci Eng A 1998;A258:99.
[45] Paris D, Lesbats P. J Nucl Mater 1978;69/70:628.
[46] Franz M. Doctoral thesis. Göttingen: Cuvillier; 1995.
[47] Riviére JP, Grilhé J. Scr Met 1975;9:967.
[48] Besson R, Morillo J. Phys Rev B 1997;55:193.
[49] Fähnle M, Mayer J, Meyer B. Intermetallics 1999;7:315.
[50] Fu CL, Ye YY, Yoo MH, Ho KM. Phys Rev B 1993;48:6712.
[51] Mayer J, Elsässer C, Fähnle M. Phys Stat Solid B 1995;191:283.
[52] Ishida S, Ishida J, Asano S, Yamashita J. J Phys Soc Jpn 1976;41:1570.